IEEE Photonics Journal
An IEEE Photonics Society Publication

Open Access

A High-Performance SiO_2/SiN_x 1-D Photonic Crystal UV Filter Used for Solar-Blind Photodetectors

Volume 11, Number 4, August 2019

Ruyue Yuan
Haifan You
Qing Cai
Kexiu Dong
Tao Tao
Bin Liu
Dunjun Chen
Rong Zhang
Youdou Zheng

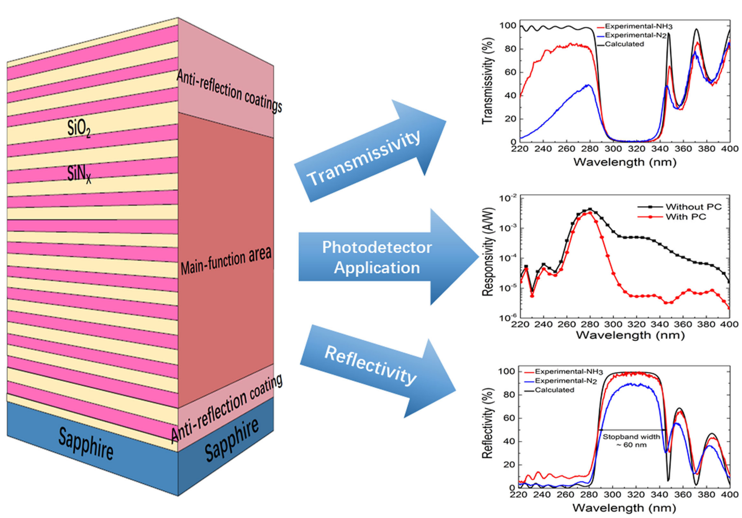

DOI: 10.1109/JPHOT.2019.2931374

IEEE photonics SOCIETY
IEEE

A High-Performance SiO_2/SiN_x 1-D Photonic Crystal UV Filter Used for Solar-Blind Photodetectors

Ruyue Yuan,[1] **Haifan You**,[1] **Qing Cai**,[1] **Kexiu Dong**,[2] **Tao Tao**,[1] **Bin Liu**,[1] **Dunjun Chen**,[1] **Rong Zhang**,[1] **and Youdou Zheng**[1]

[1]Key Laboratory of Advanced Photonic and Electronic Materials, School of Electronic Science and Engineering, Nanjing University, Nanjing 210093, China
[2]School of Mechanical and Electronic Engineering, Chuzhou University, Chuzhou 23900, China

DOI:10.1109/JPHOT.2019.2931374

Manuscript received June 10, 2019; revised July 17, 2019; accepted July 23, 2019. Date of publication July 29, 2019; date of current version August 8, 2019. This work was supported in part by the National Key R&D Program of China under Grant 2016YFB0400903, in part by the National Natural Science Foundation under Grant 61634002, in part by the NSAF under Grant U1830109, in part by the Key R&D Project and "333" project of Jiangsu Province, China under Grant BE2016174 and Grant BRA2018040, and in part by the Anhui University Natural Science Research Project, China under Grant KJ2019A0644.
Corresponding author: Dunjun Chen (e-mail: djchen@nju.edu.cn).

Abstract: To improve the solar-blind/visible-blind photocurrent response rejection ratio of solar-blind photodetectors, we designed and fabricated a high-performance SiO_2/SiN_x 1-D photonic crystal (PC) ultraviolet (UV) filter on (0 0 0 1) double-polished sapphire substrate. When depositing SiN_x, we found that employing NH_3 as nitrogen precursor instead of N_2 can simultaneously improve the peak reflectivity of filter stopband in the designed visible-blind region and the transmissivity in the solar-blind region. Research shows that it is associated with the H atom concentration in SiN_x and the generation of Si-O-N transition layer at SiO_2/SiN_x interface. Finally, we obtained a high-performance SiO_2/SiN_x PC UV filter with a stopband reflectivity over 90% from 285 to 345 nm and a transmissivity over 80% in the solar-blind region. The UV filter is also demonstrated to have a good effect in improving the solar-blind/visible-blind photocurrent response rejection ratio of a back-illuminated AlGaN photodetector by depositing it to the back of the detector.

Index Terms: Photonic crystal (PC), UV Filter, SiO_2/SiN_x, photodetectors.

1. Introduction

Solid state solar-blind ultraviolet (UV) photodetectors are attracting more and more attention because of their potential applications in civil and military fields such as engine control, UV deep space exploration, flame sensors, missile warning and secure space-to-space communication [1]–[5]. Out-of-band light response of solar-blind region is still a key problem that influences the detecting sensitivity of devices to weak solar-blind UV light ($<$290 nm) signal, although some materials, such as AlGaN and Ga_2O_3 wide bandgap semiconductors widely concerned in recent, are of characteristic of intrinsic solar-blind. Detectors made out of these materials would be sensitive only to ultraviolet light that does not penetrate the earth's atmosphere. However, defects and impurities that can result in photocurrent response from out-band of solar-blind in the wide bandgap

TABLE 1
Deposition Parameters of SiO_2 and SiN_x Layers with NH_3 and N_2 as Nitrogen Precursor, Respectively, by PECVD

Deposition material	SiO_2	SiN_x (N_2)	SiN_x (NH_3)
Growth rate/nm min^{-1}	21.41	6.52	8.95
Reaction temperature/°C	350	350	350
RF power/W	10	15	50
Reaction pressure/mTorr	300	600	500
N_2O gas flow/cm^3 min^{-1}	400	/	/
N_2 gas flow/cm^3 min^{-1}	/	900	400
NH_3 gas flow/cm^3 min^{-1}	/	900	20
SiH_4/N_2 gas flow/cm^3 min^{-1}	100	25	25

compounds are unavoidable. So the UV filters with high reflectivity in visible-blind region and high transmissivity in solar-blind region are still needed for developing the solar-blind photodetectors.

The 1-D photonic crystal (PC) filter based on SiO_2/SiN_x films can achieve very high reflectivity and wide stopband in theory because of relative large contrast of refractive index between SiO_2 and SiN_x [6]–[8]. Meanwhile, periodic SiO_2/SiN_x films can be deposited directly on the back of back-illuminated photodetectors and hence this SiO_2/SiN_x based filter can be integrated easily to the photodetector. However, it is very challenging to grow high quality SiO_2/SiN_x based 1-D PC filter with high reflectivity in the visible-blind region and transmissivity in the solar-blind region simultaneously, because solar-blind wave band is very close to their optical bandgaps of SiO_2 and SiN_x, and meanwhile reflectivity in the visible-blind region and transmissivity in the solar-blind region are two contradictory parameters that one requires more periodic layers to increase reflection to visible-blind light and the other requires less layers to decrease absorption to solar-blind light.

In this work, we designed and fabricated a 1-D PC UV filter to improve the solar-blind/visible-blind photocurrent response rejection ratio of solar-blind photodetectors, and the filter consists of periodic SiO_2/SiN_x $(L/2\ H\ L/2)_m$ units sandwiched between two anti-reflection coatings. The structure and growth parameters of the UV filter including gas sources and flow rate were optimized by means of the analysis of optical properties, microstructure, and depth profiles of atom concentration as well as theoretical calculation. Finally, we obtained a high performance SiO_2/SiN_x 1-D PC UV filter with a stopband reflectivity over 90% from 285 nm to 345 nm and a transmissivity over 80% in the solar-blind region. In addition, the actual effect in improving solar-blind/visible-blind photocurrent response rejection ratio of the UV filter was demonstrated by integrating the filter to the back of an AlGaN solar-blind photodetector.

2. Experimental

All SiO_2/SiN_x 1-D PC UV filter samples were fabricated by plasmas-enhanced chemical vapor deposition (OXFORD Plasma 80 Plus PECVD) on (0001) double-polished sapphire substrates. The silicon and oxygen precursors were SiH_4 (5%) and N_2O, respectively. For comparison, we choose N_2 [9], [10] and NH_3 [11], [12] as nitrogen precursor, respectively. Initially, the single SiN_x and SiO_2 layers were deposited respectively at the reactor to calibrate the growth rate and optical constants about refractive index (n) and extinction coefficient (k). The detailed experimental parameters are listed in Table 1. The growth rate was determined by measuring the thickness of the films using a step profiler.

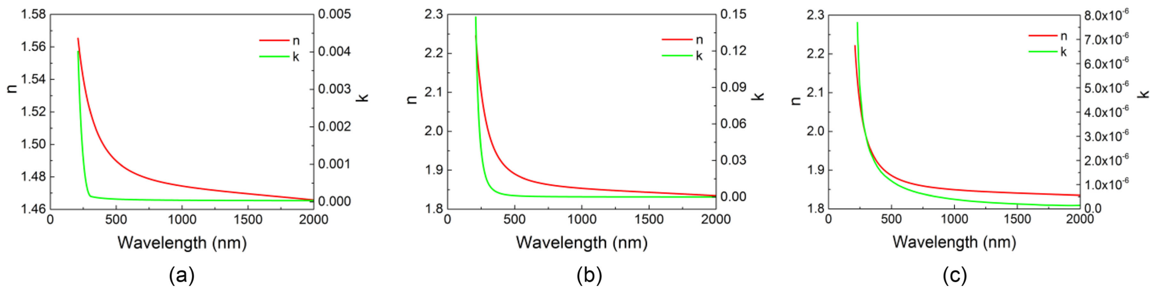

Fig. 1. Refractive index (n) and extinction coefficient (k) of SiO_2 (a) and SiN_x grown with N_2 (b) and NH_3 (c) as nitrogen precursor measured by spectroscopic ellipsometer.

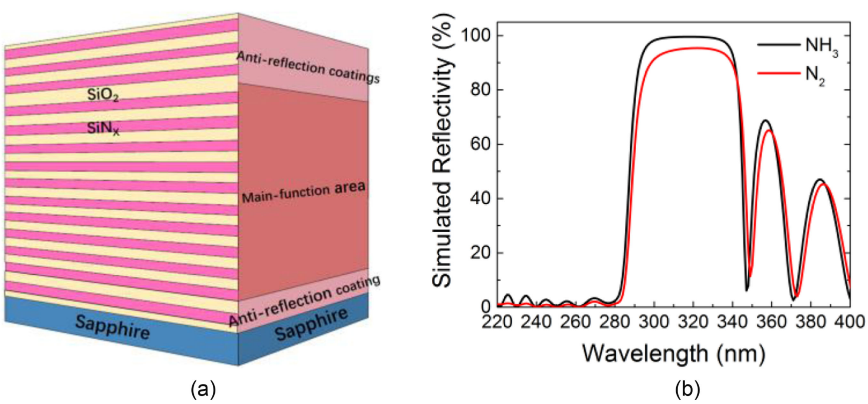

Fig. 2. Schematic diagram (a) and the calculated reflectivity spectra (b) of designed UV filters considering N_2 and NH_3 as nitrogen precursor, respectively.

In addition, the structures of UV filter were deposited according to the calibrated conditions. The reflectivity and transmissivity spectra were measured by UV-visible spectrometer (SHIMADZU UV-3600). The surface morphologies of samples were observed by atomic force microscope (NT-MDT Modular AFM). The cross-sectional images of samples were characterized by transmission electron microscope (FEI Tecnai G2 F20 S-TWIN TEM). The concentration depth profiles of elements in the samples were measured by secondary ion mass spectroscopy (PHI Adept 1010 SIMS).

3. Structure Design and Optimization

A center wavelength of 310 nm and a stopband from 290 to 350 nm are excepted for UV filters used for solar-blind photodetectors. According to this requirement, we optimized the structure of the PC UV filter by using the transfer matrix method based on the experimental optical constants of SiO_2 and SiN_x. The refractive index and extinction coefficient were measured by the EOPTICS ME-L broadband spectroscopic ellipsometer, as shown in Fig. 1(a), (b), (c). It is noteworthy that the SiN_x layer grown with NH_3 as nitrogen precursor has a significant reduction in extinction coefficient by comparing Fig. 1(b) and Fig. 1(c). The optimized structure of 1-D PC UV filter consists of the periodic main-function units $(L/2\ H\ L/2)_m$ and two anti-reflection coatings, as illustrated in Fig. 2(a). L and H represent the thickness of SiO_2 and SiN_x, respectively. The main-function units consist of 10-period $SiO_2/SiN_x/SiO_2$ layers, and the thickness of three layers is 25.5/39.3/25.5 nm calculated by

$$d = \lambda_0/4n$$

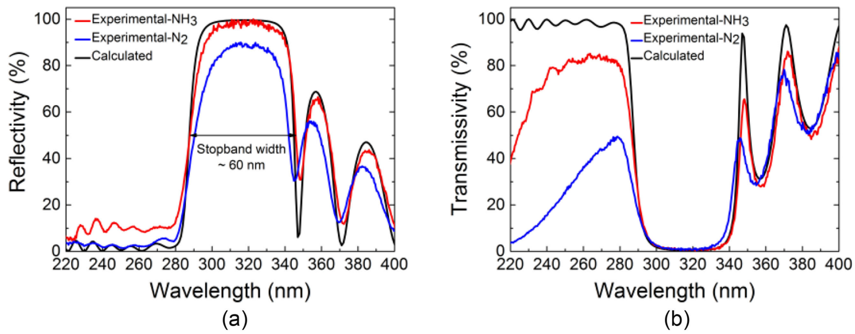

Fig. 3. The measured reflectivity (a) and transmissivity (b) spectra of the UV filters grown with NH_3 and N_2 as nitrogen precursor, respectively. The calculated reflectivity and transmissivity spectra are also presented as reference.

Two anti-reflection coatings are similar to the main-function units besides a slight change in the thickness of each layer. The top anti-reflection structure is 1.04*(L/2 H L/2)$_3$ and the bottom one is 1.35*(L/2 H L/2). The reflectivity spectra calculated by transfer matrix method and simulated by TFCalc system are shown in Fig. 2(b). The calculated spectra according to the measured optical constants show that the UV filter fabricated with NH_3 as nitrogen precursor has a higher reflectivity of approaching 100% compared to the UV filter fabricated with N_2 as nitrogen precursor. The calculated stopband covers from about 285 nm to 340 nm for both the UV filters.

4. Results and Discussion

Fig. 3 shows the actual reflectivity and transmissivity spectra of the SiO_2/SiN_x PC UV filters fabricated using different nitrogen precursors, measured by UV-visible spectrometer. The filter using NH_3 as nitrogen precursor has a higher maximum stopband peak reflectivity of 99% and a wider stopband width of 60 nm from 285 nm to 345 nm, although the reflectivity in the solar-blind region is slightly higher when comparing with that using N_2 as nitrogen precursor. It can be seen that the experimental reflectivity spectrum of the optimized UV filter is in a good coincidence with the calculated reflectivity spectrum. Furtherly, the transmissivity of the filter using NH_3 as nitrogen precursor in the solar-blind region is twice stronger than that of the filter using N_2 as nitrogen precursor, as shown in Fig. 3(b), indicating that there exists very serious light absorption in the solar-blind region for the filter using N_2 as nitrogen precursor.

To explain the causes that result in the large discrepancies on reflectivity and transmissivity of the SiO_2/SiN_x PC UV filters fabricated using different nitrogen precursors, we analyzed the element depth profiles of the two kinds of UV filters. Fig. 4(a) and (b) show depth profiles of ion concentration for Si, O, N, and H in the SiO_2/SiN_x PC UV filters grown with N_2 and NH_3 as nitrogen precursor, respectively, measured by SIMS. On the whole, depth profile curves present periodic composition fluctuations in accordance with the designed SiO_2/SiN_x bilayer structure, and the discrepancies on the ion concentrations of Si, N, and H in the SiN_x layers of the two UV filters can be observed obviously. The SiN_x layer grown with N_2 as nitrogen precursor exhibits the feature of N-rich SiN_x with a N/Si ratio of about 5:3, and has a high H atom concentration of about 16%. In contrast, the SiN_x layer grown with NH_3 as nitrogen precursor exhibits the feature of Si-rich SiN_x with a N/Si ratio of almost 1:1, and has a low H atom concentration of about 2%. To investigate the effect of intrinsic absorption from the N-rich SiN_x and Si-rich SiN_x films on the reflectivity and transmissivity spectra of the SiO_2/SiN_x PC UV filters, we extracted optical bandgap of the SiN_x films by characterizing the transmissivity spectra with the plots [13]–[15], as shown in Fig. 5. The extracted optical bandgaps are 5.14 eV and 5.31 eV for the N-rich SiN_x and Si-rich SiN_x films, respectively, corresponding to the intrinsic absorption cut-off edge of 241 nm to 234 nm. This means that the intrinsic absorption of SiN_x films has little effect on the reflectivity and transmissivity spectra of the PC UV filters in

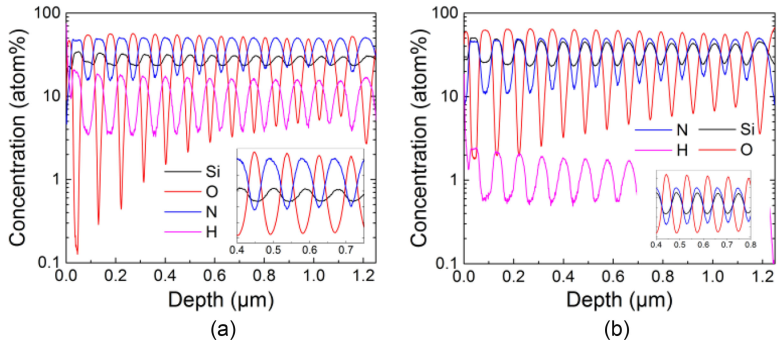

Fig. 4. Depth profile of ion concentration for Si, O, N, and H in the UV filter structure grown with N_2 (a) and NH_3 (b) as nitrogen precursor, respectively, measured by SIMS.

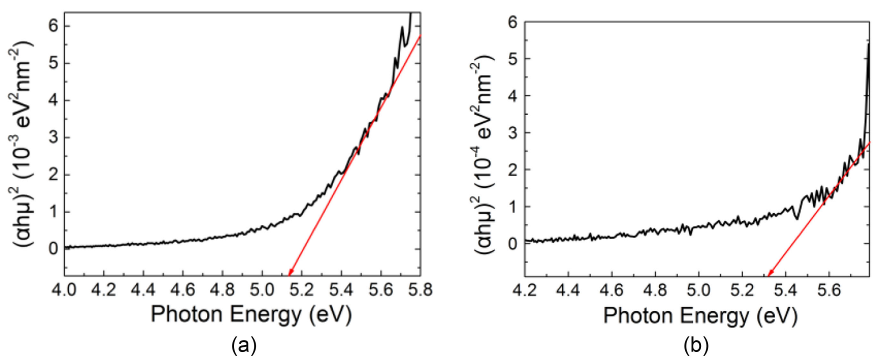

Fig. 5. The optical bandgap characterized from the transmissivity spectra of SiN_x grown with N_2 (a) and NH_3 (b) as nitrogen precursor, respectively.

the wavelength range of 240–345 nm. So, we think that the high H atom concentration in the N-rich SiN_x film is responsible for its decreasing reflectivity in the stopband and transmissivity in the solar-blind region. This can be explained by the absorption of Si-H bond to the photons with energy above 3.52 eV [16], [17], which is also in good agreement with the large discrepancy in extinction coefficient between the SiN_x films grown with NH_3 and N_2 as nitrogen precursor, respectively. However, the absorption of Si-H bond cannot explain the larger transmissivity discrepancy in the solar-blind region between two PC UV filters. This large transmissivity discrepancy can be mainly attributed to the formation of a thin Si-O-N transition layer between the SiO_2 and SiN_x layers in the PC UV filter with N_2 as nitrogen precursor. The Si-O-N transition layer with graded composition can be observed obviously from the inset of Fig. 4(a), and this transition layer was also often observed in other references [18], [19]. The Si-O-N film has an extensive range of optical bandgap from 2.9 to 6.2 eV according to different references [20], [21], and hence exists significant absorption in the solar-blind region.

$$(\alpha h\mu)^2 - h\mu$$

Fig. 6(a) and Fig. 6(b) show the surface morphology measured by AFM and cross-sectional TEM image of the SiO_2/SiN_x PC UV filter using NH_3 as nitrogen precursor. A smooth surface with altitude range less than 16 nm is observed, and the root mean square roughness is only 1.85 nm which is much lower than the structure with the similar thickness reported in recent literature [22]. In the TEM image, we can observe a 29-layer periodic structure composed of two alternating materials where the white layer represents SiO_2 and the black layer represents SiN_x. The SiO_2/SiN_x interfaces near

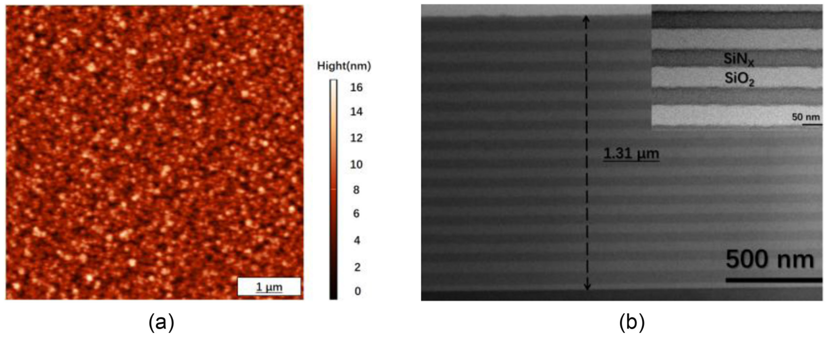

Fig. 6. Surface morphology (a) and cross-sectional image (b) of UV filter grown with NH_3 as nitrogen precursor revealed by AFM and TEM, respectively.

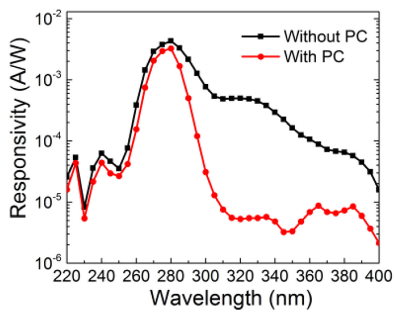

Fig. 7. Spectral responsivities of the p-$Al_{0.2}Ga_{0.8}N$/i-$Al_{0.4}Ga_{0.6}N$/n-$Al_{0.4}Ga_{0.6}N$ solar-blind photodetector under back illumination in both cases before and after depositing PC UV filter.

sapphire substrate are very clear and pretty flat, and become slightly unsmooth with the increase of the number of layers of filter as shown in the inset. The whole thickness of the UV filter measured is 1.31 μm, and the mean thicknesses of SiO_2 and SiN_x in the main function area are 51.3 nm and 39.1 nm, respectively. The measured thickness from the TEM image agrees well with the designed one with a periodic 51.0 nm/39.3 nm SiO_2/SiN_x structure.

To verify the actual effect of the SiO_2/SiN_x PC UV filter, we deposited it to the back of a traditional p-$Al_{0.2}Ga_{0.8}N$/i-$Al_{0.4}Ga_{0.6}N$/n-$Al_{0.4}Ga_{0.6}N$ solar-blind photodetector. Fig. 7 shows the photocurrent responsivity of the solar-blind photodetector under back illumination in both cases before and after depositing PC UV filter by using a calibrated monochromator and a Xe arc lamp as light source. The power of the monochromatic light was tested by a calibrated silicon. It can be seen that the spectral responsivity of the solar-blind photodetector integrated with PC UV filter presents a sharper cutoff wavelength at 285 nm and the response peak at 330 nm resulted from the photo-generated current of the p-$Al_{0.2}Ga_{0.8}N$ layer disappears in comparison with the as-fabricated solar-blind photodetector. Although the responsivity in the solar-blind region decreases slightly, the photocurrent response from out of solar-blind region is significantly suppressed by almost two orders of magnitude. We attribute the suppression of photocurrent response from out of solar-blind region to the high reflectivity of the 1-D PC UV filter in the visible-blind region.

5. Conclusion

In summary, a high performance SiO_2/SiN_x 1-D photonic crystal UV filter with stopband reflectivity over 90% from 285 nm to 345 nm and a transmissivity over 80% in the solar-blind region has been successfully fabricated by optimizing the deposition parameters and structure. This can be attributed to the significant reduction in extinction coefficient and the suppression of the generation of Si-O-N transition layer at SiO_2/SiN_x interface when using NH_3 as nitrogen precursor instead of N_2. When integrating the UV filter to the back of a AlGaN solar-blind photodetector, the photocurrent response of the detector from out of solar-blind region can be significantly suppressed by almost two orders of magnitude.

References

[1] J. Bulmer *et al.*, "Visible-blind APD heterostructure design with superior field confinement and low operating voltage," *IEEE Photon. Technol. Lett.*, vol. 28, no. 1, pp. 39–42, Jan. 2016.
[2] S. Wang *et al.*, "Efficient optical coupling in AlGaN/GaN quantum well infrared photodetector via quasi-one-dimensional gold grating," *Opt. Exp.*, vol. 23, no. 7, pp. 8740–8748, Apr. 2015.
[3] S. Choi *et al.*, "Geiger-mode operation of GaN avalanche photodiodes grown on GaN substrates," *IEEE Photon. Technol. Lett.*, vol. 20, no. 20, pp. 1526–1528, Oct. 2009.
[4] M. Gonschorek, J. F. Carlin, E. Feltin, M. A. Py, and N. Grandjean, "Self heating in AlInN/AlN/GaN high power devices: Origin and impact on contact breakdown and IV characteristics," *J. Appl. Phys.*, vol. 109, no. 6, Mar. 2011, Art. no. 063720.
[5] E. Bellotti, F. Bertazzi, S. Shishehchi, M. Matsubara, and M. Goano, "Theory of carriers transport in III-nitride materials: State of the art and future outlook," *IEEE Trans. Electron Devices*, vol. 60, no. 10, pp. 3204–3215, Oct. 2013.
[6] K. Kintaka *et al.*, "Potential characterization of free-space-wave drop demultiplexer using cavity-resonator-integrated grating input/output coupler," *Opt. Exp.*, vol. 18, no. 24, Nov. 2010, pp. 25108–25115.
[7] S. B. Bashar, M. Sujia, W. H. Shi, and J. L. Liu, "Enhanced random lasing from distributed Bragg reflector assisted Au-ZnO nanowire Schottky diode," *Appl. Phys. Lett.*, vol. 109, no. 19, Nov. 2016, Art. no. 192101.
[8] H. A. Macleod, *Thin-Film Optical Filters*. Boca Raton, FL, USA: CRC Press, 2010.
[9] V. Raghunathan, T. Izuhara, J. Michel, and L. Kimerling, "Stability of polymer-dielectric bi-layers for athermal silicon photonics," *Opt. Exp.*, vol. 20, no. 14, pp. 16059–16066, Jul. 2012.
[10] S. C. Mao *et al.*, "Low propagation loss SiN optical waveguide prepared by optimal low-hydrogen module," *Opt. Exp.*, vol. 16, no. 25, pp. 20809–20816, Dec. 2008.
[11] E. Mon-Perez *et al.*, "Experimental and theoretical rationalization of the growth mechanism of silicon quantum dots in non-stoichiometric SiN_x: role of chlorine in plasma enhanced chemical vapour deposition," *Nanotechnology*, vol. 27, no. 45, Nov. 2016, Art. no. no. 455703.
[12] A. Y. Liu, Z. Hameiri, Y. M. Wan, C. Sun, and D. Macdonald, "Gettering effects of silicon nitride films from various plasma-enhanced chemical vapor deposition conditions," *IEEE J. Photovolt.*, vol. 9, no. 1, pp. 78–81, Jan. 2019.
[13] J. Tauc, R. Grigorovici, and A. Vancu, "Optical properties and electronic structure of amorphous germanium," *Phys. Status Solidi B*, vol. 15, no. 2, pp. 627–637, 1966.
[14] J. Tauc, *Amorphous and Liquid Semiconductors*. Berlin, Germany: Springer Science & Business Media, 2012.
[15] J. Tauc, "Optical properties and electronic structure of amorphous Ge and Si," *Mater. Res. Bull.*, vol. 3, no. 1, pp. 37–46, 1968.
[16] P. Nachtigall, K. D. Jordan, and K. C. Janda, "Calculation of the Si–H bond energies for the monohydride phase of Si (100)," *J. Chem. Phys.*, vol. 95, no. 11, pp. 8652–8654, Dec. 1991.
[17] Y. R. Luo, *Handbook of Bond Dissociation Energies in Organic Compounds*. Boca Raton, FL, USA: CRC Press, 2002.
[18] M. Schaepkens *et al.*, "Study of the SiO_2-to-Si_3N_4 etch selectivity mechanism in inductively coupled fluorocarbon plasmas and a comparison with the SiO_2-to-Si mechanism," *J. Vac. Sci. Technol. A*, vol. 17, no. 1, pp. 26–37, Jan.–Feb. 1999.
[19] L. U. J. T. Ogbuji and S. R. Bryan, "The SiO_2-Si_3N_4 interface, Part 1: Nature of the interphase," *J. Amer. Ceram. Soc.*, vol. 78, no. 5, pp. 1272–1278, May 1995.
[20] Z. W. Lin *et al.*, "The role of N–Si–O defect states in optical gain from an a-SiN_xO_y/SiO_2 waveguide and in light emission from an n-a-SiN_xO_y/p-Si Heterojunction LED," *Phys. Status Solidi A*, vol. 215, no. 12, Jun. 2018, Art. no. 1700750.
[21] H. P. Ma *et al.*, "Measurements of microstructural, chemical, optical, and electrical properties of silicon-oxygen-nitrogen films prepared by plasma-enhanced atomic layer deposition," *Nanomaterials*, vol. 8, no. 12, Dec. 2018, Art. no. 1008.
[22] J. P. Dai *et al.*, "Design and fabrication of UV band-pass filters based on SiO_2/Si_3N_4 dielectric distributed Bragg reflectors," *Appl. Surf. Sci.*, vol. 364, pp. 886–891, Feb. 2016.